Article

Journal of the Brazilian Chemical Society

https://dx.doi.org/10.21577/0103-5053.20240014

J. Braz. Chem. Soc. **2024**, *35*, 7, e-20240014, 1-11

Investigating Solvent-Induced Changes in Structure and Nonlinear Optical Behavior of Thiazine Derivatives

Clodoaldo Valverde, [*,a,b] ***André D. da Silva,*** [a] ***Krishna M. Potla,*** [c] ***Heibbe C. B. de Oliveira,*** [d] ***Francisco A. P. Osório*** [e,f] ***and Basílio Baseia*** [f,g]

[a]*Laboratório de Modelagem Molecular Aplicada e Simulação (LaMMAS), Universidade Estadual de Goiás, 75001-970 Anápolis-GO, Brazil*

[b]*Universidade Paulista, 74845-090 Goiânia-GO, Brazil*

[c]*Department of Chemistry, Velagapudi Ramakrishna Siddhartha Engineering College, Kanuru, Vijayawada, Andhra Pradesh 520007, India*

[d]*Laboratório de Estrutura Eletrônica e Dinâmica Molecular (LEEDMOL), Instituto de Química, Universidade Federal de Goiás, 74690-900 Goiânia-GO, Brazil*

[e]*Pontifícia Universidade Católica de Goiás, 74605-220 Goiânia-GO, Brazil*

[f]*Instituto de Física, Universidade Federal de Goiás, 74690-900 Goiânia-GO, Brazil*

[g]*Departamento de Física, Universidade Federal da Paraíba, 58051-970 João Pessoa-PB, Brazil*

In this study, we examine the effects of solvent media on the structural and optical behaviors of two isomers of thiazine derivatives: rac-2-(4-nitrophenyl)-3-phenyl-2,3,5,6-tetrahydro-4*H*-1,3-thiazin-4-one and (2*S*)-2-(3-nitrophenyl)-3-phenyl-2,3,5,6-tetrahydro-4*H*-1,3-thiazin-4-one. The solvent effects were modeled using the polarizable continuum model through density functional theory. Electrical parameters for rac-2-(4-nitrophenyl)-3-phenyl-2,3,5,6-tetrahydro-4*H*-1,3-thiazin-4-one and (2*S*)-2-(3-nitrophenyl)-3-phenyl-2,3,5,6-tetrahydro-4*H*-1,3-thiazin-4-one were determined using the density functional theory at the CAM-B3LYP/6-311+G(d) level. We studied the influence of isomer structures in various solvent media on the Hyper-Rayleigh-Scattering first hyperpolarizability, considering both static and dynamic scenarios. This research particularly emphasizes the implications of relocating the NO_2 group from the *meta*-position (2*S*)-2-(3-nitrophenyl)-3-phenyl-2,3,5,6-tetrahydro-4*H*-1,3-thiazin-4-one to the *para*-position rac-2-(4-nitrophenyl)-3-phenyl-2,3,5,6-tetrahydro-4*H*-1,3-thiazin-4-one on molecular geometries, linear and nonlinear optical parameters, and gap energies across different solvent media. Bond dissociation energy calculations for hydrogen atoms and all other single acyclic bonds were performed for both derivatives to assess degradation and autoxidation properties. Additional insights from non-bonding orbitals, molecular electrostatic surface potential, Fukui calculations, electron localization function, and localized orbital locator are detailed.

Keywords: Hyper-Rayleigh-Scattering first hyperpolarizability, electrostatic surface potential, electron localization function, localized orbital locator

Introduction

In recent years, organic materials have garnered significant attention from the scientific community, especially in the domain of nonlinear optical (NLO) properties. Their synthetic flexibility facilitates the design and production of new materials, further enhanced by theoretical modeling.[1] Unlike inorganic counterparts, organic materials, owing to their π conjugation and delocalized electronic structure, are easy to manipulate, allowing precise control over their NLO properties. They have emerged as promising candidates for studying optical nonlinearity.[2-12] The demand for materials with NLO properties has surged due to their potential applications in photonics,[13] spectroscopy,[14] optical keys,[15] ultra-fast optical

*e-mail: valverde@ueg.br
Editor handled this article: Paula Homem-de-Mello (Associate)

communications,[13] frequency converters,[16] electro-optical modulators, and more.[17] Thiazines and their derivatives are at the forefront, finding applications as efficient NLO materials,[18,19] solar cells,[20] chemical sensors,[21] and organic light-emitting diodes.[22,23] These derivatives are both electroactive and photoactive, suitable for molecular electronics.[24,25] Moreover, thiazines have therapeutic potential, being used as bioactive groups for various disease treatments[26] and in tranquilizers and insecticides.[27] They also exhibit antifungal, anti-tubercular, and antidiabetic properties.[28]

In this study, we investigate the solvent medium effects on the optical properties of two thiazine derivative isomers, synthesized and characterized by Yennawar *et al.*,[29] rac-2-(4-nitrophenyl)-3-phenyl-2,3,5,6-tetrahydro-4*H*-1,3-thiazin-4-one (RNTP) and (2*S*)-2-(3-nitrophenyl)-3-phenyl-2,3,5,6-tetrahydro-4*H*-1,3-thiazin-4-one (SNTP). Both share the same molecular formula ($C_{16}H_{14}N_2O_3S$), differing only in the position of the NO_2 group on the benzene ring, from *para* (RNTP) to *meta* (SNTP) positions (Figure 1). We employed the polarizable continuum model (PCM)[30-38] through density functional theory (DFT) to model the solvent media. The electrical parameters, including first and second hyperpolarizabilities, total dipole moment, and average linear polarizability, were computed using DFT/CAM-B3LYP with the 6-311+G(d) basis set[39-43] across multiple solvent media. Additionally, the static and dynamic Hyper-Rayleigh Scattering (HRS) first hyperpolarizability was examined based on the dielectric constant of the solvent media. This work delves into how solvent media influence the molecular geometries, linear and nonlinear optical (NLO) parameters, and gap energies of RNTP and SNTP.

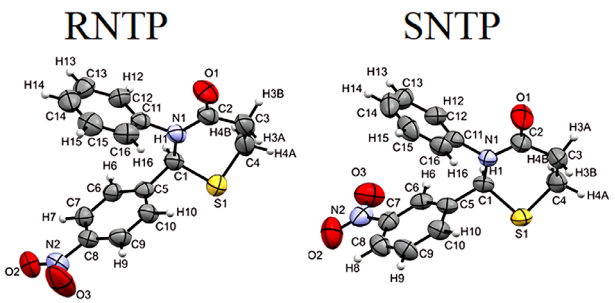

Figure 1. Molecular structures of RNTP and SNTP adapted from reference 29.

Methodology

Solvent media

The electric properties of the compounds were analyzed both in the gas-phase and in various solvent media, as detailed in Table 1. We modeled the solvent media using the PCM model at DFT/B3LYP/6-311+G(d) level. Solvent media can be broadly categorized as polar (either protic or aprotic) and nonpolar.[44] Solubility is inherently tied to the polarity of a solvent medium. In this study, we use the normalized transition energy scale (E_T^N) defined by Dimroth and Reichardt[45] to quantify the concept of polarity. The E_T^N-value is determined by the transition energy for the solvatocromic absorption band of the longest wavelength of the dye pyridinium *N*-phenolate betaine, as presented in Table 2. Any solvent with a dielectric constant (ε) below 5 is categorized as nonpolar.

Table 1. Solvent medium parameters: normalized transition energy scale (E_T^N), static dielectric constant (ε) and classification as protic or aprotic[46]

Solvent	E_T^N	ε	
Water	1.00	78.36	protic
Formamide	0.78	108.94	protic
Methanol	0.76	32.61	protic
Formic acid	0.73	51.10	protic
n-Methyl formamide-mixture	0.72	181.56	protic
Ethanol	0.65	24.85	protic
1-Butanol	0.59	17.33	protic
Acetonitrile	0.46	35.69	aprotic
Dimethyl sulfoxide (DMSO)	0.44	46.83	aprotic
2-Methyl-2propanol	0.39	12.47	protic
Acetone	0.36	20.49	aprotic
Dichloroethane	0.33	10.13	aprotic
Dichloromethane	0.31	8.93	aprotic
Chloroform	0.26	4.71	nonpolar
Tetrahydrofuran	0.21	7.43	aprotic
Chlorobenzene	0.19	5.70	aprotic
Toluene	0.10	2.37	nonpolar
Heptane	0.012	1.91	nonpolar

Molecular structure analysis

The optimized geometries of the RNTP and SNTP molecules, both in the gas phase and in different solvent media, were assessed using the root mean square deviation (RMSD). This compared the overlap between the crystalline structure determined by X-ray and those in the presence of solvent media. Additionally, angles and torsion angles were analyzed across all solvent media to understand the impact of the NO_2 group's positional shift on these structural parameters.

Frontiers molecular orbital

Using DFT/CAM-B3LYP/6-311+G(d), we determined the energies of the frontier molecular orbitals, HOMO (highest occupied molecular orbital) and LUMO (lowest unoccupied molecular orbital). The stability of the compounds RNTP and SNTP in solvent media correlates with the energy gap, defined as the difference between HOMO (electron donor) and LUMO (electron acceptor) energies. The propensity of a compound to donate or accept electrons is linked to the magnitudes of these energies.[47]

NBO, MESP, ELF and LOL methods

We employed the NBO 7.0 program[48] for Natural Bond Orbital (NBO) analysis using the 6-311+G(d) basis set, facilitated by the Gaussian software.[49] This provides an optimal foundation for analyzing Lewis-type NBOs (donors) and non-Lewis NBOs (acceptors) within a system. The NBO method allows for the examination of hyperconjugative interactions arising from electron transfers from filled bonding (donor) orbitals to vacant antibonding (acceptor) orbitals and gauging their energetic significance. Additionally, we carried out molecular electrostatic surface potential (MESP) and bond dissociation energy calculations using the DFT/CAM-B3LYP/6-311+G(d) method.[50-52] The Electron Localization Function (ELF) and Localized Orbital Locator (LOL) calculations and analyses were performed with the Multiwfn program.[53] For calculating the Fukui function, hardness, and softness, we utilized the UCA-FUKUI program,[54] which accepts Gaussian files as inputs.

Nonlinear optical properties

The electrical parameters of the thiazine derivatives studied here were calculated at DFT/CAM-B3LYP/6-311+G(d) level of theory. The dipole moment and the linear polarizability were calculated using the equations,

$$\mu = (\mu_x^2 + \mu_y^2 + \mu_z^2)^{\frac{1}{2}} \quad (1)$$

where μ is total dipole moment of the molecule and μ_x, μ_y, μ_z; are the components of the dipole moment in the x, y, and z directions, respectively.

$$\alpha = \frac{\alpha_{xx} + \alpha_{yy} + \alpha_{zz}}{3} \quad (2)$$

where ⟨α⟩ is average linear polarizability of the molecule and α_{xx}, α_{yy}, α_{zz}; are the linear polarizability components along the x, y, and z axes, respectively.

The total first hyperpolarizability is given by,

$$\beta_{tot} = (\beta_x^2 + \beta_y^2 + \beta_z^2)^{\frac{1}{2}} \quad (3)$$

where β_{tot} is the total first hyperpolarizability of the molecule and the β_x, β_y, β_z are components of the first hyperpolarizability in the x, y, and z directions, respectively.

$$\beta_i = \frac{1}{3}\sum_j (\beta_{ijj} + \beta_{jij} + \beta_{jji}) \quad (4)$$

The individual component (β_i) of the first hyperpolarizability. The mixed derivatives of the polarizability (β_{ijj}, β_{jij}, β_{jji}), indicating the change in polarizability due to the application of an electric field in different directions.

The Hyper-Rayleigh Scattering (HRS) is an experimental method used to measure the first hyperpolarizability in solution. The HRS method gives details of the nonlinear optical properties at the molecular level.[55] The HRS first hyperpolarizability (β_{HRS}) is defined by,

$$\beta_{HRS} = \sqrt{\beta_{ZZZ}^2 + \beta_{XZZ}^2} \quad (5)$$

where $\langle \beta_{XZZ}^2 \rangle$ and $\langle \beta_{ZZZ}^2 \rangle$ are macroscopic means of Hyper-Rayleigh Scattering, which are calculated through the components (β_{ijk}) of the first hyperpolarizability[35] as follows,

$$\langle \beta_{ZZZ}^2 \rangle = \frac{1}{210}\left(30\delta_1 + 12\left(\delta_2 + \delta_3 + \delta_5\right) + 6\left(\delta_4 + \delta_6\right) + 2\left(\delta_7 + \delta_8 + \delta_{11}\right) + 4\delta_9 + \delta_{10}\right) \quad (6)$$

$$\langle \beta_{XZZ}^2 \rangle = \frac{1}{210}\left(6\left(\delta_1 - \delta_3 - \delta_5 + \delta_7\right) + 8\delta_2 + 18\delta_4 + 4\delta_6 - \delta_8 - 2\delta_9 + 3\delta_{10} - \delta_{11}\right) \quad (7)$$

where the δ_n coefficients are defined in Table 2.

The average second hyperpolarizability ⟨γ⟩ is given by,

$$\langle \gamma \rangle = \frac{1}{15}\sum_{ij=x,y,z} (\gamma_{iijj} + \gamma_{ijji} + \gamma_{ijij}) \quad (8)$$

The components γ_{iijj}, γ_{ijji}, γ_{ijij} of the second hyperpolarizability tensor represent different ways the electric field can interact with the molecule to induce a nonlinear optical response.

Using the Kleymann symmetry, for the static case the ⟨γ⟩-value can be written through in the following expression,

Table 2. HRS first hyperpolarizability coefficients

$\delta_1 = \sum_i \beta_{iii}^2$	$\delta_2 = \sum_{i,j} \beta_{iii}\beta_{ijj}$
$\delta_3 = \sum_{i,j} \beta_{iii}(\beta_{jij} + \beta_{jji})$	$\delta_4 = \sum_{i,j} \beta_{ijj}^2$
$\delta_5 = \sum_{i,j} \beta_{ijj}(\beta_{jij} + \beta_{jji})$	$\delta_6 = \sum_{i,j} (\beta_{jij} + \beta_{jji})^2$
$\delta_7 = \sum_{i,j,k} \beta_{ijj}\beta_{ikk}$	$\delta_8 = \sum_{i,j,k} (\beta_{jij} + \beta_{jji})(\beta_{kik} + \beta_{kki})$
$\delta_9 = \sum_{i,j,k} \beta_{ijj}(\beta_{kik} + \beta_{kki})$	$\delta_{10} = \sum_{i,j,k} (\beta_{ijk} + \beta_{ikj})^2$
$\delta_{11} = \sum_{i,j,k} (\beta_{ijk} + \beta_{ikj})(\beta_{jjk} + \beta_{jki})$	

$$\langle\gamma\rangle = \frac{1}{5}[\gamma_{xxxx} + \gamma_{yyyy} + \gamma_{zzzz} + 2(\gamma_{xxyy} + \gamma_{xxzz} + \gamma_{yyzz})] \quad (9)$$

The terms γ_{xxxx}, γ_{yyyy} and γ_{zzzz} represent the second hyperpolarizability components when the electric field is applied four times along the same axis (x, y, or z, respectively). Meanwhile, γ_{xxyy}, γ_{xxzz} and γ_{yyzz} are mixed second hyperpolarizability components, where the electric field is applied twice in one direction and twice in another.

The Gaussian 09[49] computational package was used to perform all the calculations. The selection of the B3LYP[56-59] functional for geometry optimization and the CAM-B3LYP[60] functional for investigating non-linear optical properties is a strategic decision, reflecting the distinct strengths inherent to each functional. B3LYP is renowned for its efficiency and reliability in yielding precise molecular geometries. In contrast, CAM-B3LYP is advantageous in the characterization of phenomena involving excited states and long-range interactions, which are pivotal in the study of non-linear optical properties.[61]

In the literature,[62] the utilization of CAM-B3LYP is detailed for examining the non-linear optical properties of photochromic materials. This exemplifies the functional's pertinence for such inquiries. Notably, in the same study, geometry optimization is conducted using the B3LYP level of theory, underscoring its application in achieving optimized molecular configurations.

Results and Discussion

Solvent medium effects on the geometric properties of the compounds

We studied the solvent medium effects on the molecular properties of RNTP and SNTP using the PCM through DFT at the B3LYP/6-311+G(d) level. Nineteen solvent media (with dielectric constants, ε, ranging from 1.43 to 181.56) and the gas-phase (ε = 1) were included in the calculations.

Table S1 in the Supplementary Information (SI) section presents the RMSD values, highlighting the overlap between the X-ray-determined crystal structure (Figure 1) and those obtained in various solvent media for RNTP and SNTP. The table also features the RMSD results for the gas phase. For RNTP, the RMSD values range from 0.3316 in the gas phase to 0.3154 in *n*-methylformamide-mixture, with maximal atomic distances of 0.7311 and 0.6607 Å, respectively. In contrast, for SNTP, the RMSD values span from 0.2893 in *n*-methylformamide-mixture to 0.2388 in the gas phase, accompanied by maximum atomic distances of 0.5669 and 0.4327 Å, respectively. Figure 2 delineates the evolution of the RMSD values for RNTP and SNTP in relation to the static dielectric constant (ε) of the solvent media. For SNTP, the RMSD values increase consistently with a rise in the ε-value. However, for RNTP, RMSD values decline with increasing ε-values up to ε = 40. Beyond ε = 40, there is subtle oscillation observed in the RMSD values. This differential trend in RMSD as a function of ε can be attributed to the shift of the NO_2 group from the *para*-position (in RNTP) to the *meta*-position (in SNTP) on the benzene ring, as visualized in Figure 1.

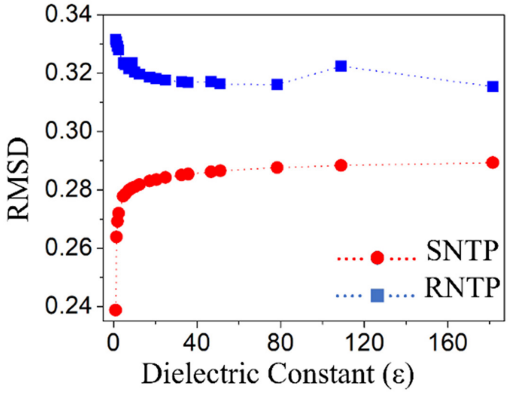

Figure 2. Evolution of the RMSD parameter for the compounds as function of the ε.

Figure 3 shows the overlap between the asymmetric unit of the crystal and the optimized geometry in formamide for RNTP and SNTP, the anchorage point is the benzene ring.

The presence of the solvent medium affects the molecular geometry of the compounds. This effect is evident in the changes in specific angles: N1–C11–C12, N1–C2–O1, S1–C1–C5, O3–N2–C8, and O3–N2–C7 across various solvent media, as documented in Table S2 (SI section). When juxtaposing the X-ray determined angles with those procured in different solvent media, the disparities are generally within a 2% range. Nonetheless,

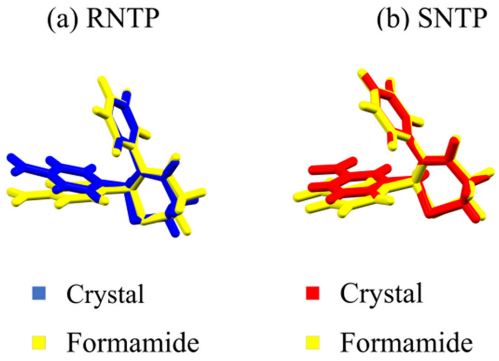

Figure 3. Overlap between the X-ray determined geometry and the optimized geometry in formamide for (a) RNTP and (b) SNTP.

the torsion angles exhibit pronounced variations when exposed to different solvent media, as delineated in Table S3 (SI section). A detailed examination of Table S3 reveals that SNTP, especially, undergoes substantial torsion angle shifts in the presence of solvent media. A case in point is the N1–C1–S1–C4 torsion angle, which shifts from an X-ray value of −59.3 to −46.1° in *n*-methylformamide-mixture, marking a percentage change of 29%.

Gap energies

Figure S3 (SI section) illustrates the variations in gap energies derived from the differences between the HOMO and LUMO energies for RNTP and SNTP across various solvent media and the gas-phase. There is a noticeable trend: as the dielectric constant (ε-value) of the solvent medium rises, the gap energy diminishes for both compounds. Specifically, the smallest recorded gap energies for RNTP and SNTP are 3.90 and 3.64 eV, respectively, both observed in *n*-methylformamide-mixture. In contrast, the peak values in the gas phase are 4.12 eV for RNTP and 3.98 eV for SNTP. For a comprehensive breakdown, one can consult Table S4 in the SI section. Intriguingly, all identified gap energies across these solvent media fall within the ultraviolet spectrum. Moving on, Figure S4 (SI section) offers a visual portrayal of the HOMO and LUMO frontier molecular orbitals, specifically for RNTP in formamide and SNTP in *n*-methyl formamide-mixture.

Natural Bond Orbital (NBO) analysis

The NBO 7.0 program[48,53] was used for NBO analysis at 6-311G+(d) basis set, which is executed in Gaussian software which offers a suitable basis for analysis of Lewis-type NBOs (donor) and non-Lewis NBOs (acceptor) interactions in a system. The larger the stabilization energy value E(2), revealed the most effective filled and empty interactions. The perturbation energy values of the important Lewis-type NBOs (donor) and non-Lewis NBOs (acceptor) interactions are tabulated in Tables S5 and S6 (SI section).

For the molecule RNTP, the very strong interaction n3O2→π*(N2-O3) has the highest E(2) value, 164 kcal mol^{-1}, strong interactions have been in n1N1→ π*(C2-O1) and n2O1→σ*(C2-N1) with energies of 42.26 and 26.85 kcal mol^{-1} respectively. Tables S7 and S8 (SI section) give the occupancy of electrons and p-character[37] in significant NBO natural atomic hybrid orbital. Almost 100% p-character was observed in π-bonding of C2–O1, C5–C6, C11–C12, N2–03 and the lone pairs of n1N1, n2O1, n2O2, n3O2, n2O3 and n2S1.

For the molecule, SNTP the very strong interaction n3O2→π*(N2-O3) has the highest E(2) value, 163.37 kcal mol^{-1}, strong interactions have been in n1N1→(C2-O1) and n2O1→σ*(C2-N1) with the energies of 38.81 and 26.76 kcal mol^{-1} respectively. Almost 100% p-character was observed in π-bonding of C2–O1, C5–C6, C11–C12, N2–03 and the lone pairs of n1N1, n2O1, n2O3, n3O2, n2O2 and n2S1.

The interactions, n3O2→π*(N2-O3) = 164 kcal mol^{-1} (SNTP) and n3O2→π*(N2-O3) = 163.37 kcal mol^{-1} (RNTP) are expected due to resonance effect within the nitro group. Other interactions, n1N1→ π*(C2-O1) = 42.26 (SNTP) and n1N1→(C2-O1) = 38.81 kcal mol^{-1} (RNTP) are due to lone pair of electrons on the nitrogen atom is delocalized into the carbonyl group. The afore mentioned interactions lead to a high degree of stabilization of the title molecules.

Local reactivity properties analysis

The three-dimensional rainbow color-coded depiction of molecular electrostatic surface potential (MESP) for RNTP and SNTP is illustrated in Figures S1 and S2, as provided in the SI section. This quantum chemical phenomenon, which is based on electron density, offers insights into reactive sites, hydrogen bonding, and biological activity. Electron-rich regions, depicted in red, are susceptible to electrophilic attacks, whereas electron-poor regions, shown in blue, are prone to nucleophilic attacks. To predict the specific areas of a molecule vulnerable to electrophilic, nucleophilic, and radical attacks, scientists employ the Fukui function. Introduced by Parr and Yang,[63] in 1984, this function considers the addition or removal of electrons, accounting for variations in charge and multiplicity. The calculations for the Fukui function are based on the following equations:

$$f^- = [q(N) - q(N - 1)]; \text{ for an electrophilic attack} \quad (10)$$

$$f^+ = [q(N + 1) - q(N)]; \text{ for a nucleophilic attack} \quad (11)$$

$f^0 = [q(N + 1) – q(N – 1)]/2$for a radical attack (12)

If N signifies the total of electrons, then N + 1 relates to an anion and N –1 relates to the cation of the molecule.[64] The calculations are performed at the ground state by using the B3LYP/6-311+G(d) level of theory.

Dual descriptor proposed by Morell *et al.*[65] represent with a symbol Δf(r), which is obtained as the contrast between the nucleophilic (f^+) and electrophilic (f^-) Fukui function is represented by:

$$\Delta f(r) = (f^+(r)) – (f^-(r)) \quad (13)$$

Δf(r) values are represented with Δf(r) < 0 (negative, – ve) symbol indicates the electrophilic attack and Δf(r) > 0 (positive, + ve) symbol indicates the nucleophilic attack.

From the molecular electrostatic surface potential and dual-descriptor Δf(r) analysis (Tables S9 and S10, SI section) we observed that the region which is more prone to the electrophilic attack (which is denoted with red color on MESP and Δf(r) negative value) was around the S1 = –0.2648, O1 = –0.1434 and N1 = –0.1201 (RNTP); S1 = –0.2003, O1 = –0.1446 and N1 = –0.1686 (SNTP). While N2 = 0.2579 (RNTP) and N2 = 0.2762 (SNTP) susceptible towards nucleophilic attack and has Δf(r) positive value.

Electron Localization Function (ELF) and Localized Orbital Locator (LOL)

In a molecular, or atomic, system the estimation of localization of electrons and localized electron cloud have been studied through the ELF and LOL approach based on the kinetic energy density, helpful for characterizing chemical bonds.[66-69] The two-dimensional graphical representations of the color filled and counter maps of ELF and LOL for RNTP and SNTP are shown in Figures 4 and 5.

Color-filled ELF plots are displayed using a rainbow color scheme. Here, the red color represents maximum Pauli repulsion, with a value of 1, and is predominantly seen over hydrogen atoms. In contrast, the blue color, signifying a minimum with a value of 0, is observed over oxygen, sulfur, nitrogen, and carbon atoms. In the color-filled LOL plots utilizing the same rainbow scheme, covalent regions are depicted in red and are associated with a value of 1. Meanwhile, the regions showcasing electron depletion between the valence shell and the inner shell are represented in blue, indicating a value of 0.[12]

Sensitivity towards autoxidation

Calculation of hydrogen-bond dissociation energy (H-BDE) and bond dissociation energy (BDE)

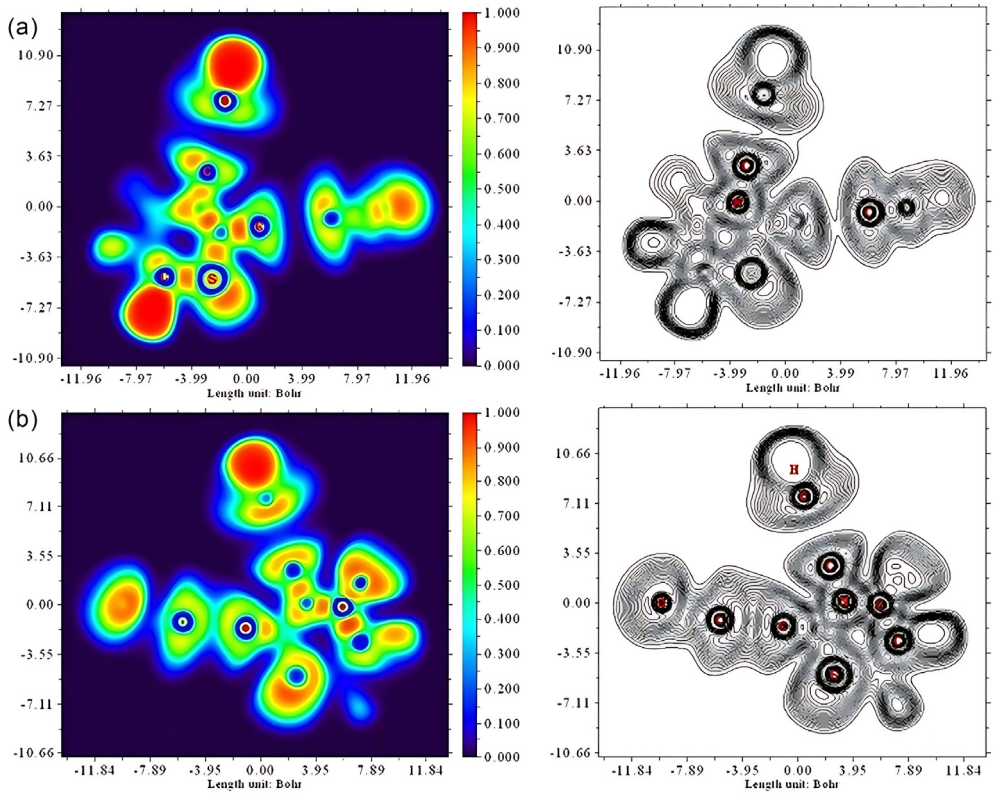

Figure 4. Electron Localization Function (ELF) color filled and contour map of SNTP (a) and RNTP (b) molecules.

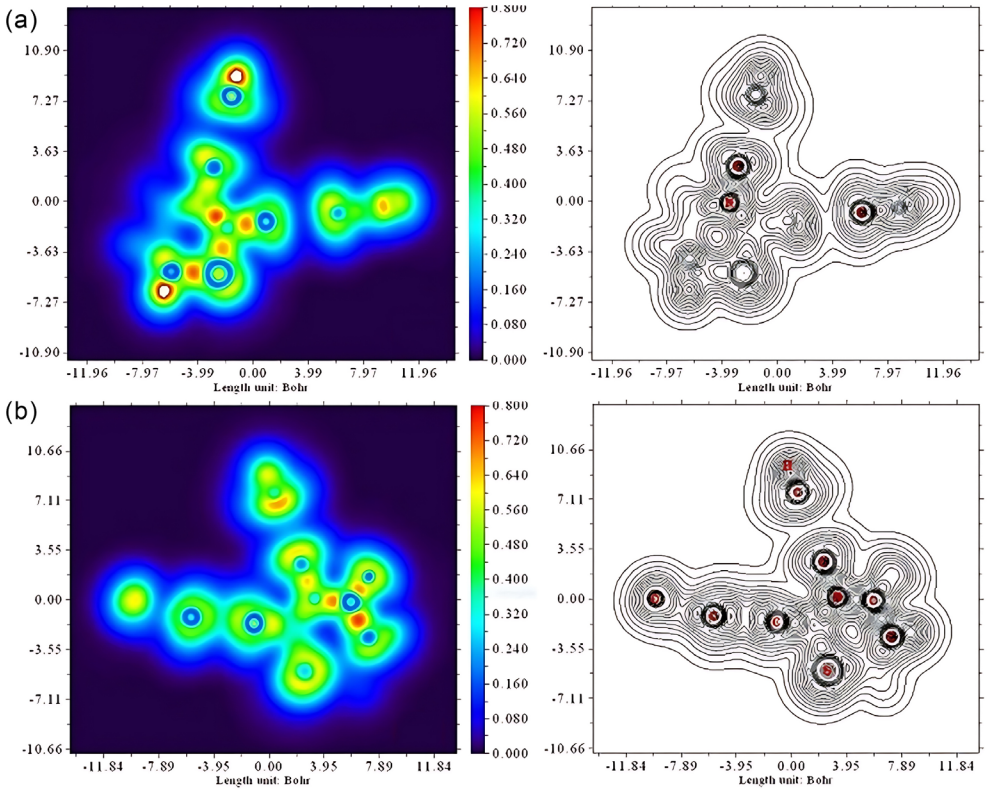

Figure 5. Localized Orbital Locator (LOL) color filled and contour map of SNTP (a) and RNTP (b) molecules.

values plays a great role in the field of pharmaceutical drug development due to the below mentioned reasons. Namely, the C–H bonds were cleaved in phase I drug metabolism through the hydroxylation process.[70,71] Another one, the calculations of the H-BDE and BDE allow the assessment of the possibility of a drug candidate to give deterioration products while being put away.[72,73] Calculation of H-BDE and BDE values are very important from both therapeutic and environmental aspects, the calculations, we have carried out are denoted in Figure S5 (SI section). From literature,[70,74] studies revealed that H-BDE values between 70-85 kcal mol^{-1} were sensitivity towards the autooxidation process.

The H-BDE values are greater than 85 kcal mol^{-1} for the present investigated compounds RNTP and SNTP, which showed that could not be subtle towards the autoxidation process. BDE values are calculated for all the single acyclic bonds for the investigated compounds, and the results revealed that the deterioration could start precisely by cleavage of C8–N2 bond for RNTP (BDE value for C8–N2 bond 65.88 kcal mol^{-1}) and C7–N2 bond for SNTP (BDE value for C7–N2 bond 65.88 kcal mol^{-1}).

Non-linear optical parameters

In this section, we examine the impact of solvent media on the electrical parameters of RNTP and SNTP. To understand how solvents influence the electrical properties of RNTP and SNTP, we analyzed the electrical charges in atoms in both the gas phase and solvent medium. This analysis employed the PCM method and the CHELPG electrostatic model, calculated via DFT (CAM-B3LYP/6-311+G(d)). Detailed findings are presented in Tables S11 and S12 (SI section).

Figure 6 presents the dipole moment (μ) as a function of the static dielectric constant of various solvent media. For both compounds, the μ-value increases with the rise in the ε-value. From argon to *n*-methylformamide-mixture, the percentage increase in μ-value is more pronounced for RNTP

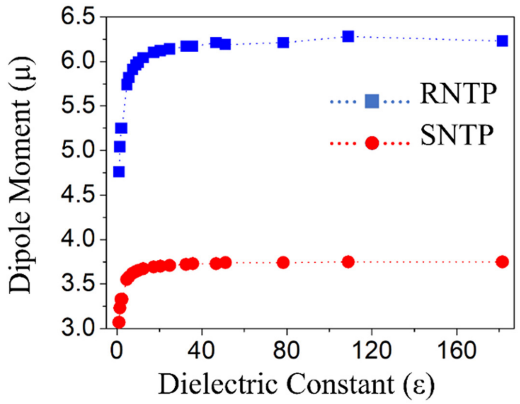

Figure 6. Dipole moment as function of the dielectric constant of the solvent media.

(24.6%) than for SNTP (16.1%). For both compounds, when $\varepsilon \geq 40$, the dipole moment approaches saturation.

In formamide, RNTP exhibits a dipole moment 67.47% higher than SNTP in the same solvent. This disparity can be attributed to the following: the total charge of the group (C5–H10–C10–C9–H9–C8–H7–C7–C6–H6–N2–O2–O3) is 0.0971e for RNTP and 0.1031e for SNTP. Meanwhile, for the group (C2–C3–H3B–H4B–H3A–H4A–C4–S1–C1–H1–N1–O1), the total charge is –0.3534e for RNTP and –0.3500e for SNTP. RNTP has a more substantial charge separation than SNTP, which directly impacts the total dipole moment.

The results for the electrical properties average linear polarizability ($\langle\alpha(0; 0)\rangle$), first hyperpolarizability parallel to dipole moment ($\beta_{\|}z(0; 0,0)$) and the average second hyperpolarizability ($\langle\gamma(0; 0,0,0,)\rangle$) as function of the ε-value are shown in the Figure 7. As can be seen, all the functions for both compounds show a monotonic increase in the electric parameter with the increasing dielectric constant, and a saturation for high ε-values ($\varepsilon \geq 40$). The percentage increase of the average linear polarizability and of the average second hyperpolarizability for RNTP and SNTP are similar ca. 31 and 39% for $1.43 < \varepsilon < 181.56$. However, the absolute value of $\beta_{\|}z(0; 0,0)$ for RNTP presents an increasing of 452% (from 0.23×10^{-30} esu to 1.27×10^{-30} esu), and of 170% (from 1.10×10^{-30} esu to 2.97×10^{-30} esu) for SNTP.

Figure 8 shows the results for β_{HRS} as function of the frequency ($0.0 < \omega < 0.10$ a.u.) of the electric field for only four solvent media namely, formamide ($\varepsilon = 108.94$), water ($\varepsilon = 78.36$), chloroform ($\varepsilon = 4.71$), and DMSO ($\varepsilon = 46.83$). From Figure 6 can be seen that the resonant frequencies regions for the compounds occur for $\omega > 0.08$ a.u., thus we will work away from the resonance region, that is, we will work with $\omega = 0.0428$ a.u.

Tables S13 and S14 (SI section) show the β_{HRS}-values for RNTP and SNTP in several solvent media. Particularly in formamide, the obtained values for the RNTP (SNTP) in the cases static and dynamic with $\omega = 0.0428$ a.u. were $\beta_{HRS}^{static} = 8.63 \times 10^{-30}$ esu ($\beta_{HRS}^{static} = 5.52 \times 10^{-30}$ esu) and $\beta_{HRS}^{dynamic} = 8.84 \times 10^{-30}$ esu ($\beta_{HRS}^{dynamic} = 5.19 \times 10^{-30}$ esu), respectively. The $\beta_{HRS}^{dynamic}$ of the compound RNTP in the solvent formamide presents the highest value among all the solvents for the frequency $\omega = 0.0428$ a.u. and this can be explained because in this solvent we have the lowest gap energy value (see Figure S3, SI section).

The ratio between for RNTP and the β_{HRS} for SNTP (named β_{HRS}-ratio) as function of the dielectric constant of the solvent medium is shown in Figure S6 (SI section), in both cases, static and dynamic ($\omega = 0.0428$ a.u.).

The change of the NO_2 group from the *meta*-position (SNTP) to the *para*-position (RNTP) at the benzene ring (Figure 1) influences significantly the NLO responses of the compounds. As can be seen in Figure S6, the ratio between the HRS hyperpolarizability of RNTP and SNTP is always greater than the unit, and β_{HRS}-ratio-value increases (decreases) with the increasing of the ε-value for the dynamic (static) case for $\varepsilon \leq 108.94$ (formamide).

The β_{HRS}-values at $\omega = 0.0428$ a.u. for RNTP and SNTP in chloroform are 1.06 times and 0.64 times the value for *p*-nitroaniline (*p*NA), that is a molecule commonly used as the external reference ($\beta_{HRS}^{\omega = 0.0428} = 7.2 \times 10^{-30}$ esu).[51]

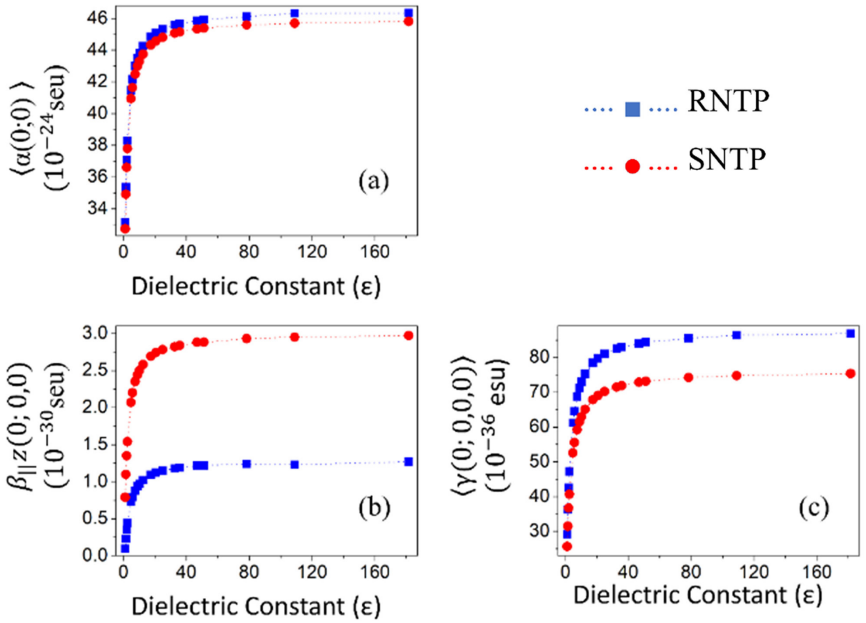

Figure 7. Static electric parameters for the RNTP and SNTP as function of the dielectric constant of the solvent medium.

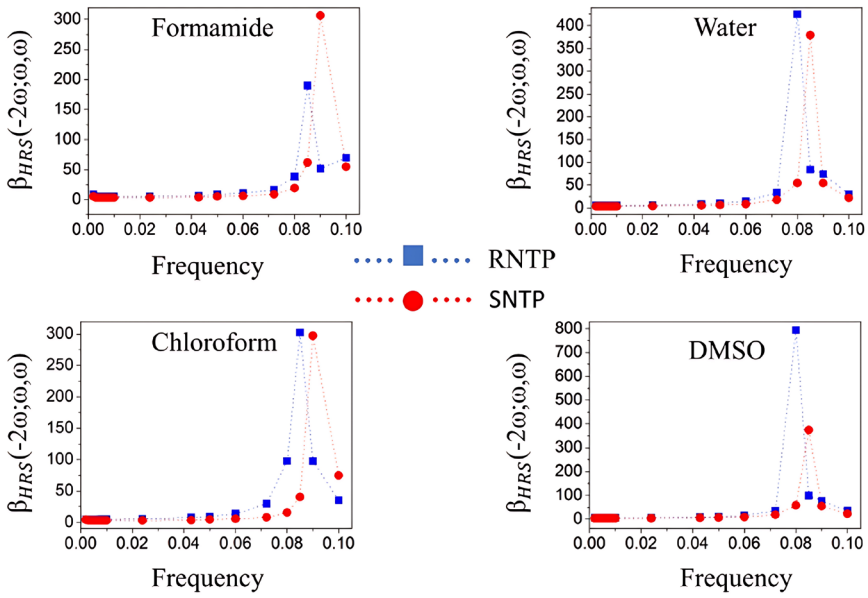

Figure 8. Dynamic HRS first hyperpolarizability as function of the electric field frequency (a.u.) in some solvent media.

Conclusions

In this study, the effects of solvent media on the structural, linear, and nonlinear optical properties of two isomeric thiazine derivatives, RNTP and SNTP, were explored. The distinguishing feature between these molecules is the positioning of the NO_2-group on the benzene ring: either in the *para*-position or *meta*-position. Using PCM/DFT theory, the optimized molecular structures of these compounds were simulated in various solvent media.

We assessed the congruence between X-ray coordinates and optimized coordinates in the solvent medium using the RMSD method. Energy values from hydrogen bond dissociation showed that both SNTP and RNTP molecules resist autoxidation. However, the low bond dissociation energy for the C–N bond suggests that the degradation mechanism may initiate with this bond's cleavage. According to MESP and the Fukui dual-descriptor, the most likely centers for electrophilic attack are the carbonyl oxygen (O1), sulfur (S1), and nitrogen atoms (N1).

DFT/CAM-B3LYP/6-311+G(d) results indicate that static electrical parameters for both compounds in various solvents increase as the dielectric constant of the solvents rises. While the static values of the dipole moment, average linear polarizability, and average second hyperpolarizability for RNTP surpass those for SNTP, SNTP has higher values for parallel first hyperpolarizability.

Additionally, an analysis was conducted on the first hyperpolarizability of both the static and dynamic Hyper-Rayleigh Scattering (HRS) concerning the dielectric constant of the solvent. RNTP values consistently exceeded those for SNTP across all solvents. Thus, relocating the NO_2-group from *para*-position to *meta*-position in the compounds notably influences their optical properties, and this shift is modulated by the properties of the solvent medium. From a structural perspective, the most noticeable modification in molecules immersed in solvent media pertains to the torsion angles of SNTP. This modification carries an impact on the optical properties of the compound.

Supplementary Information

Supplementary information is available free of charge at http://jbcs.sbq.org.br as PDF file.

Acknowledgments

The authors would like to thank the following Brazilian agencies for financial support: Conselho Nacional de Desenvolvimento Científico e Tecnológico (CNPq), Coordenação de Aperfeiçoamento Pessoal de Nível Superior (CAPES); Pró-reitoria de Pesquisa e Pós-Graduação da PUC-GO (Prope) and Fundação de Apoio à Pesquisa do Estado de Goiás (FAPEG). Research developed with support of the High-Performance Computing Center at the Universidade Estadual de Goiás (UEG).

Author Contributions

Clodoaldo Valverde led the conceptualization, methodology, and investigation, and was also responsible for writing the original draft; André D. da Silva was involved in data curation and validation, and he also contributed to the review and editing process; Krishna

M. Potla focused on experimental design and data analysis, while also assisting in writing the original draft; Heibbe C. B. de Oliveira contributed to the methodology and data curation, and he too took part in the writing and review process; Francisco A. P. Osório provided essential laboratory infrastructure and resources, and participated in the manuscript's review phase. Lastly, Basílio Baseia played a pivotal role in supervising and coordinating the project, securing funding, and also engaged in the review and editing of the manuscript. Together, these authors collaborated effectively to bring the research to fruition and prepare the manuscript for publication.

References

1. Jothi, L.; Vasuki, G.; Babu, R. R.; Ramamurthi, K.; *Optik* **2014**, *125*, 2017. [Crossref]
2. Valverde, C.; Osório, F. A. P.; Fonseca, T. L.; Baseia, B.; *Chem. Phys. Lett.* **2018**, *706*, 170. [Crossref]
3. Srivastava, R.; Al-Omary, F. A. M.; El-Emam, A. A.; Pathak, S. K.; Karabacak, M.; Narayan, V.; Chand, S.; Prasad, O.; Sinha, L.; *J. Mol. Struct.* **2017**, *1137*, 725. [Crossref]
4. Manivannan, S.; Tiwari, S. K.; Dhanuskodi, S.; *Solid State Commun.* **2004**, *132*, 123. [Crossref]
5. Nayak, S. K.; Kore, R.; Ahmed, M. S.; Verma, P.; Vallavoju, R.; Banerjee, D.; Pola, S.; Soma, V. R.; Chetti, P.; Raavi, S. S. K.; *Opt. Mater.* **2023**, *137*, 113603. [Crossref]
6. Santos, F. A.; Cardoso, C. E. R.; Rodrigues, J. J.; De Boni, L.; Abegão, L. M. G.; *Photonics* **2023**, *10*, 545. [Crossref]
7. Nath, S.; Puthukkudi, A.; Mohapatra, J.; Biswal, B. P.; *Angew. Chem.* **2023**, *135*, e202218974. [Crossref]
8. Alagumalai, A.; Sahu, S. S.; Lourderaj, U.; Vijayasayee, S. M.; Krishnamoorthy, A.; Thangavelu, S. A. G.; *New J. Chem.* **2023**, *47*, 17951. [Crossref]
9. El-Khouly, M. E.; Kobaisy, A. M.; Ahmed, H.; El-Hendawy, M. M.; Ghali, M.; El-Said, W. A.; Al-Bogami, A. S.; Mohamed, T.; *Opt. Quantum Electron.* **2023**, *55*, 941. [Crossref]
10. Borges, I. D.; Danielli, J. A. V.; Silva, V. E. G.; Sallum, L. O.; Queiroz, J. E.; Dias, L. D.; Iermak, I.; Aquino, G. L. B.; Camargo, A. J.; Valverde, C.; Osório, F. A. P.; Baseia, B.; Napolitano, H. B.; *RSC Adv.* **2020**, *10*, 22542. [Crossref]
11. Custodio, J. M. F.; Santos, F. G.; Vaz, W. F.; Cunha, C. E. P.; Silveira, R. G.; Anjos, M. M.; Campos, C. E. M.; Oliveira, G. R.; Martins, F. T.; da Silva, C. C.; Valverde, C.; Baseia, B.; Napolitano, H. B.; *J. Mol. Struct.* **2018**, *1157*, 210. [Crossref]
12. Potla, K. M.; Poojith, N.; Osório, F. A. P.; Valverde, C.; Chinnam, S.; Suchetan, P. A.; Vankayalapati, S.; *J. Mol. Struct.* **2020**, *1210*, 128070. [Crossref]
13. Lu, L.; Liang, Z.; Wu, L.; Chen, Y.; Song, Y.; Dhanabalan, S. C.; Ponraj, J. S.; Dong, B.; Xiang, Y.; Xing, F.; Fan, D.; Zhang, H.; *Laser Photonics Rev.* **2018**, *12*, 1700221. [Crossref]
14. Luo, M.; Liang, F.; Song, Y.; Zhao, D.; Xu, F.; Ye, N.; Lin, Z.; *J. Am. Chem. Soc.* **2018**, *140*, 3884. [Crossref]
15. Nakano, M.; *Chem. Rec.* **2017**, *17*, 27. [Crossref]
16. Shi, G.; Wang, Y.; Zhang, F.; Zhang, B.; Yang, Z.; Hou, X.; Pan, S.; Poeppelmeier, K. R.; *J. Am. Chem. Soc.* **2017**, *139*, 10645. [Crossref]
17. Mendonça, C. R.; Misoguti, L.; Dall' Agnol, F. F.; Zilio, S. C.; *Rev. Bras. Ensino Fis.* **1999**, *2*, 272. [Crossref]
18. Vipin Das, K. G.; Yohannan Panicker, C.; Narayana, B.; Nayak, P. S.; Sarojini, B. K.; Al-Saadi, A. A.; *Spectrochim. Acta, Part A* **2015**, *135*, 162. [Crossref]
19. Moustafa, H.; Elshakre, M. E.; Elramly, S.; *J. Mol. Struct.* **2017**, *1136*, 25. [Crossref]
20. Wong, W.-Y.; Chow, W.-C.; Cheung, K.-Y.; Fung, M.-K.; Djurišić, A. B.; Chan, W.-K.; *J. Organomet. Chem.* **2009**, *694*, 2717. [Crossref]
21. Hauck, M.; Schönhaber, J.; Zucchero, A. J.; Hardcastle, K. I.; Müller, T. J. J.; Bunz, U. H. F.; *J. Org. Chem.* **2007**, *72*, 6714. [Crossref]
22. Kim, G. W.; Cho, M. J.; Yu, Y.-J.; Kim, Z. H.; Jin, J.-I.; Kim, D. Y.; Choi, D. H.; *Chem. Mater.* **2007**, *19*, 42. [Crossref]
23. Cho, N. H.; Jang, H. C.; Park, H. K.; Cho, Y. W.; *Diabetes Res. Clin. Pract.* **2006**, *71*, 177. [Crossref]
24. Sailer, M.; Nonnenmacher, M.; Oeser, T.; Müller, T. J. J.; *Eur. J. Org. Chem.* **2006**, *2006*, 423. [Crossref]
25. Sailer, M.; Franz, A. W.; Müller, T. J. J.; *Chem. - Eur. J.* **2008**, *14*, 2602. [Crossref]
26. Sadigh, M. K.; Zakerhamidi, M. S.; *Opt. Laser Technol.* **2018**, *100*, 216. [Crossref]
27. Bolotin, P. A.; Baranovsky, S. F.; Evstigneev, M. P.; *Spectrochim. Acta, Part A* **2006**, *64*, 693. [Crossref]
28. Mooibroek, T. J.; Gamez, P.; *Inorg. Chim. Acta* **2007**, *360*, 381. [Crossref]
29. Yennawar, H. P.; Bradley, H. G.; Perhonitch, K. C.; Reppert, H. E.; Silverberg, L. J.; *Acta Crystallogr., Sect. E: Crystallogr. Commun.* **2018**, *74*, 454. [Crossref]
30. Miertuš, S.; Scrocco, E.; Tomasi, J.; *Chem. Phys.* **1981**, *55*, 117. [Crossref]
31. Miertuš̃, S.; Tomasi, J.; *Chem. Phys.* **1982**, *65*, 239. [Crossref]
32. Pascual-ahuir, J. L.; Silla, E.; Tuñon, I.; *J. Comput. Chem.* **1994**, *15*, 1127. [Crossref]
33. Tomasi, J.; Persico, M.; *Chem. Rev.* **1994**, *94*, 2027. [Crossref]
34. Cancès, E.; Mennucci, B.; Tomasi, J.; *J. Chem. Phys.* **1997**, *107*, 3032. [Crossref]
35. Cossi, M.; Barone, V.; Mennucci, B.; Tomasi, J.; *Chem. Phys. Lett.* **1998**, *286*, 253. [Crossref]
36. Tomasi, J.; Cammi, R.; Mennucci, B.; Cappelli, C.; Corni, S.; *Phys. Chem. Chem. Phys.* **2002**, *4*, 5697. [Crossref]
37. Tomasi, J.; *Theor. Chem. Acc.* **2004**, *112*, 184. [Crossref]
38. Tomasi, J.; Mennucci, B.; Cammi, R.; *Chem. Rev.* **2005**, *105*, 2999. [Crossref]
39. Krishnan, R.; Binkley, J. S.; Seeger, R.; Pople, J. A.; *J. Chem. Phys.* **1980**, *72*, 650. [Crossref]

40. Clark, T.; Chandrasekhar, J.; Spitznagel, G. W.; Schleyer, P. V. R.; *J. Comput. Chem.* **1983**, *4*, 294. [Crossref]
41. Feller, D.; *J. Comput. Chem.* **1996**, *17*, 1571. [Crossref]
42. Schuchardt, K. L.; Didier, B. T.; Elsethagen, T.; Sun, L.; Gurumoorthi, V.; Chase, J.; Li, J.; Windus, T. L.; *J. Chem. Inf. Model.* **2007**, *47*, 1045. [Crossref]
43. Pritchard, B. P.; Altarawy, D.; Didier, B.; Gibson, T. D.; Windus, T. L.; *J. Chem. Inf. Model.* **2019**, *59*, 4814. [Crossref]
44. Hoffmann, A.; Leininger, S.; Regitz, M.; *J. Organomet. Chem.* **1997**, *539*, 61. [Crossref]
45. Reichardt, C.; *Chem. Rev*. **1994**, *94*, 2319. [Crossref]
46. Valverde, C.; Batista Soares, J. V.; Duarte da Silva, A.; Vieira da Luz, B.; Almeida dos Santos, D. J.; Barbosa Carvalho, E. G.; Monteiro Oliveira, Y. C.; Barbosa Napolitano, H.; Baseia, B.; Pinto Osório, F. A.; *Rev. Colomb. Quim.* **2020**, *49*, 33. [Crossref]
47. Wang, S. R.; Arrowsmith, M.; Böhnke, J.; Braunschweig, H.; Dellermann, T.; Dewhurst, R. D.; Kelch, H.; Krummenacher, I.; Mattock, J. D.; Müssig, J. H.; Thiess, T.; Vargas, A.; Zhang, J.; *Angew. Chem., Int. Ed.* **2017**, *56*, 8009. [Crossref]
48. Glendening, E. D.; Landis, C. R.; Weinhold, F.; *J. Comput. Chem.* **2019**, *1*, 25873. [Crossref]
49. Frisch, M. J.; Trucks, G. W.; Schlegel, H. B.; Scuseria, G. E.; Robb, M. A.; Cheeseman, J. R.; Scalmani, G.; Barone, V.; Mennucci, B.; Petersson, G. A.; Nakatsuji, H.; Caricato, M.; Li, X.; Hratchian, H. P.; Izmaylov, A. F.; Bloino, J.; Zheng, G.; Sonnenberg, J. L.; Hada, M.; Ehara, M.; Toyota, K.; Fukuda, R.; Hasegawa, J.; Ishida, M.; Nakajima, T.; Honda, Y.; Kitao, O.; Nakai, H.; Vreven, T.; Montgomery, J. A.; Peralta, J. E.; Ogliaro, F.; Bearpark, M.; Heyd, J. J.; Brothers, E.; Kudin, K. N.; Staroverov, V. N.; Keith, T.; Kobayashi, R.; Normand, J.; Raghavachari, K.; Rendell, A.; Burant, J. C.; Iyengar, S. S.; Tomasi, J.; Cossi, M.; Rega, N.; Millam, J. M.; Klene, M.; Knox, J. E.; Cross, J. B.; Bakken, V.; Adamo, C.; Jaramillo, J.; Gomperts, R.; Stratmann, R. E.; Yazyev, O.; Austin, A. J.; Cammi, R.; Pomelli, C.; Ochterski, J. W.; Martin, R. L.; Morokuma, K.; Zakrzewski, V. G.; Voth, G. A.; Salvador, P.; Dannenberg, J. J.; Dapprich, S.; Daniels, A. D.; Farkas, O.; Foresman, J. B.; Ortiz, J. V; Cioslowski, J.; Fox, D. J.; Montgomery Jr., J. A.; Peralta, J. E.; Ogliaro, F.; Bearpark, M.; Heyd, J. J.; Brothers, E.; Kudin, K. N.; Staroverov, V. N.; Kobayashi, R.; Normand, J.; Raghavachari, K.; Rendell, A.; Burant, J. C.; Iyengar, S. S.; Tomasi, J.; Cossi, M.; Rega, N.; Millam, J. M.; Klene, M.; Knox, J. E.; Cross, J. B.; Bakken, V.; Adamo, C.; Jaramillo, J.; Gomperts, R.; Stratmann, R. E.; Yazyev, O.; Austin, A. J.; Cammi, R.; Pomelli, C.; Ochterski, J. W.; Martin, R. L.; Morokuma, K.; Zakrzewski, V. G.; Voth, G. A.; Salvador, P.; Dannenberg, J. J.; Dapprich, S.; Daniels, A. D.; Farkas, Ö.; Foresman, J. B.; Ortiz, J. V.; Cioslowski, J.; Fox, D. J.; *Gaussian, Revision 09,* Gaussian Inc., Wallingford, CT, USA, 2013. [Crossref]
50. Custodio, J. M. F.; Ternavisk, R. R.; Ferreira, C. J. S.; Figueredo, A. S.; Aquino, G. L. B.; Napolitano, H. B.; Valverde, C.; Baseia, B.; *J. Phys. Chem. A* **2019**, *123*, 153. [Crossref]
51. Custodio, J. M. F.; D'Oliveira, G. D. C.; Gotardo, F.; Cocca, L. H. Z.; de Boni, L.; Perez, C. N.; Napolitano, H. B.; Osorio, F. A. P.; Valverde, C.; *Phys. Chem. Chem. Phys.* **2021**, *23*, 6128. [Crossref]
52. Custodio, J. M. F.; Moreira, C. A.; Valverde, C.; de Aquino, G. L. B.; Baseia, B.; Napolitano, H. B.; *J. Braz. Chem. Soc.* **2017**, *29*, 257. [Crossref]
53. Lu, T.; Chen, F.; *J. Comput. Chem.* **2012**, *33*, 580. [Crossref]
54. Sánchez-Márquez, J.; Zorrilla, D.; Sánchez-Coronilla, A.; de los Santos, D. M.; Navas, J.; Fernández-Lorenzo, C.; Alcántara, R.; Martín-Calleja, J.; *J. Mol. Model.* **2014**, *20*, 2492. [Crossref]
55. Bersohn, R.; Pao, Y.; Frisch, H. L.; *J. Chem. Phys.* **1966**, *45*, 3184. [Crossref]
56. Becke, A. D.; *J. Chem. Phys.* **1993**, *98*, 5648. [Crossref]
57. Lee, C.; Yang, W.; Parr, R. G.; *Phys. Rev. B* **1988**, *37*, 785. [Crossref]
58. Vosko, S. H.; Wilk, L.; Nusair, M.; *Can. J. Phys.* **1980**, *58*, 1200. [Crossref]
59. Stephens, P. J.; Devlin, F. J.; Chabalowski, C. F.; Frisch, M. J.; *J. Phys. Chem.* **1994**, *98*, 11623. [Crossref]
60. Yanai, T.; Tew, D. P.; Handy, N. C.; *Chem. Phys. Lett.* **2004**, *393*, 51. [Crossref]
61. Valverde, C.; Medeiros, R.; Franco, L. R.; Osório, F. A. P.; Castro, M. A.; Fonseca, T. L.; *Sci. Rep.* **2023**, *13*, 8616. [Crossref]
62. Sutradhar, T.; Misra, A.; *RSC Adv.* **2020**, *10*, 40300. [Crossref]
63. Yang, W.; Parr, R. G.; Pucci, R.; *J. Chem. Phys.* **1984**, *81*, 2862. [Crossref]
64. Kolandaivel, P.; Praveena, G.; Selvarengan, P.; *J. Chem. Sci.* **2005**, *117*, 591. [Crossref]
65. Morell, C.; Grand, A.; Toro-Labbé, A.; *J. Phys. Chem. A* **2005**, *109*, 205. [Crossref]
66. Becke, A. D.; Edgecombe, K. E.; *J. Chem. Phys.* **1990**, *92*, 5397. [Crossref]
67. Poater, J.; Duran, M.; Solà, M.; Silvi, B.; *Chem. Rev.* **2005**, *105*, 3911. [Crossref]
68. Silvi, B.; Savin, A.; *Nature* **1994**, *371*, 683. [Crossref]
69. Jacobsen, H.; *Can. J. Chem.* **2008**, *86*, 695. [Crossref]
70. Drew, K. L. M.; Reynisson, J.; *Eur. J. Med. Chem.* **2012**, *56*, 48. [Crossref]
71. Ortiz de Montellano, P. R.; *Chem. Ver.* **2010**, *110*, 932. [Crossref]
72. Andersson, T.; Broo, A.; Evertsson, E.; *J. Pharm. Sci.* **2014**, *103*, 1949. [Crossref]
73. Lienard, P.; Gavartin, J.; Boccardi, G.; Meunier, M.; *Pharm. Res.* **2015**, *32*, 300. [Crossref]
74. Gryn'ova, G.; Hodgson, J. L.; Coote, M. L.; *Org. Biomol. Chem.* **2011**, *9*, 480. [Crossref]

Submitted: August 29, 2023
Published online: January 29, 2024